ACS OMEGA

http://pubs.acs.org/journal/acsodf

Article

Analysis of the Biochemical Reaction Status by Real-Time Monitoring Molecular Diffusion Behaviors Using a Transistor Biosensor Integrated with a Microfluidic Channel

Yao-Hsuan Lai, Jin-Chun Lim, Ya-Chu Lee, and Jian-Jang Huang*

Cite This: *ACS Omega* 2021, 6, 11911−11917

Read Online

ACCESS | Metrics & More | Article Recommendations

ABSTRACT: Traditional methods of monitoring biochemical reactions measure certain detectable reagents or products while assuming that the undetectable species follow the stoichiometry of the reactions. Here, based upon the metal-oxide thin-film transistor (TFT) biosensor, we develop a real-time molecular diffusion model to benchmark the concentration of the reagents and products. Using the nicotinamide adenine dinucleotide (NADH)−oxaloacetic acid with the enzyme of malate dehydrogenase as an example, mixtures of different reagent concentrations were characterized to extract the ratio of remaining concentrations between NAD^+ and NADH. We can thus obtain the apparent equilibrium constant of the reaction, $(8.06 \pm 0.61) \times 10^4$. Because the whole analysis was conducted using a TFT sensor fabricated using a semiconductor process, our approach has the advantages of exploring biochemical reaction kinetics in a massively parallel manner.

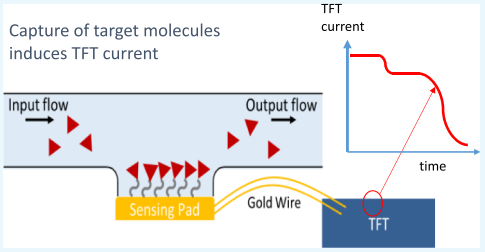

1. INTRODUCTION

The analysis of biochemical reactions is important for molecular biology research and is critical for tissue distribution, the metabolism, and drug discovery.[1−6] Biomaterials or biochemical reactions are usually monitored from measurable reagents or products by methods such as gas monitoring,[7] colorimetric determination,[8,9] and pH detection.[10] However, not all reactants and products in the reaction are detectable due to the limitation of the measurement method. The concentration of the undetectable material is derived by calculating the concentration of the detectable substance based on the stoichiometric coefficients. In addition, biochemical reactions are often mediated by catalysts or stoichiometric reactants, which affect the reaction rates. Slight errors in the measurement of the concentrations of reactants and products may cause distortions in the calculated equilibrium constants. Sophisticated measurement and analysis methods are required to enhance the accuracy.

Transistor-based biosensors have been widely studied in detecting proteins, ligands, nucleotides, and cells.[11−15] Because most reactants or products in the biochemical reactions carry electrical charges, transistor-based biosensors are very sensitive in detecting target analytes in the reactions. They were also employed for monitoring the kinetics of biochemical reactions, in which the complete and incomplete reactions, the equilibrium coefficient, and the reaction rate can be obtained.[16−18] The abovementioned approaches of extracting the concentrations of target analytes or reaction parameters were often conducted by establishing their correlations with transistor parameter changes, such as variations of current, threshold voltage, and so forth. For example, we previously analyzed the lysozyme and tri-*N*-acetyl-D-glucosamine (NAG_3) reaction kinetics by monitoring the thin-film transistor (TFT) drain current change with the molecular concentration.[18] Target analytes are recognized from the specific time drain currents start to change.[15] However, the accuracy of determining the concentration of target analytes becomes a big challenge because the single-parameter changes are very sensitive to the environmental interference, instability of the sensing devices, and improper design of the experimental flow.

In this paper, a new approach is proposed to study the biochemical reaction kinetics. We employed a molecular diffusion model to correlate the concentration of molecules detected and the drain current response of the TFT-microfluidic biosensor. Instead of extracting the transistor current difference at a specific time target molecules arrived at the sensing pad, this work monitors the current change profile when molecules diffuse through the microfluidic channel over a period of time. We demonstrate the applicability of the biosensor on extracting the equilibrium constant of nicotinamide adenine dinucleotide, reduced form (NADH)−oxalo-

Received: January 13, 2021
Accepted: March 24, 2021
Published: April 2, 2021

acetic acid (OAA, the conjugate acid of oxaloacetate) with its catalyst, malate dehydrogenase (MDH),[19,20] without labeling or immobilization. Even though the lack of a cross-linker may lead to a higher limit of detection, the diffusion behavior of biomolecules in the microfluidic channel will be less affected so that more accurate results can be obtained.

2. RESULTS AND DISCUSSION

2.1. Bare Chip Current Response. Under the condition that the microfluidic channel is prefilled with only phosphate-buffered saline (PBS) (pH 7.4), the transient response of the bare chip is shown in Figure 1. The drain current first decreases because the amorphous layers of the device are under a constant electrical stress, which is attributed to the device defects in the indium−gallium−zinc oxide (IGZO) channel, gate dielectric, and thin-film interfaces,[21] and the ionic redistribution in solution.[22] Also shown in Figure 1 is the instability of drain current caused by the injection. A sudden change of drain current is observed at around 50−100 s after 0.01 × PBS is injected. The time interval between the injection and response detected using the TFT is nearly independent of the microfluidic channel length adopted in our design. Therefore, for the subsequent experiment, the length of the microfluidic channel is chosen to be 7.9 mm (excluding the 6.1 mm-in-diameter inject inlet) to ensure that target molecules arrive at the sensing pad much longer than the injection turbulence.

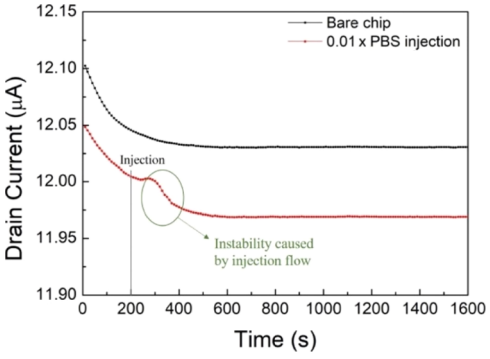

Figure 1. Transient drain current profile of a bare TFT with the microfluidic channel filled with PBS (black line). The current response profile of the TFT when the 0.01 × PBS solution is injected to the microfluidic channel at t = 200 s (red line) is shown. The corresponding turbulence occurs at around 250−350 s.

2.2. Real-Time Analysis of NADH and NAD$^+$ Molecules Diffusing toward the Sensing Pad. In the next step, we separately measured and analyzed the drain current responses of NADH and NAD$^+$ solutions with the concentrations of 10, 3.33, 1, and 0.33 mM. When the target analyte arrives at the sensing pad, the drain current changes correspondingly. The drain current response of each solution is shown in Figure 2a,b. The decrease of drain current at t = 200−300 s is caused by the turbulence of the injection (see Figure 1), while the signal at t > 1000 s is induced by the target molecules. Since both NADH and NAD$^+$ biomolecules carry negative charges under pH 7.4, the mobile molecules arrive at the Au metal plate (without cross-linkers) and deplete negative charges in the upper side of the transistor channel, leading to the decrease of drain current. The trend of current change is opposite to the case in which cross-linkers are employed to capture target molecules.[18] When the positive-charged target

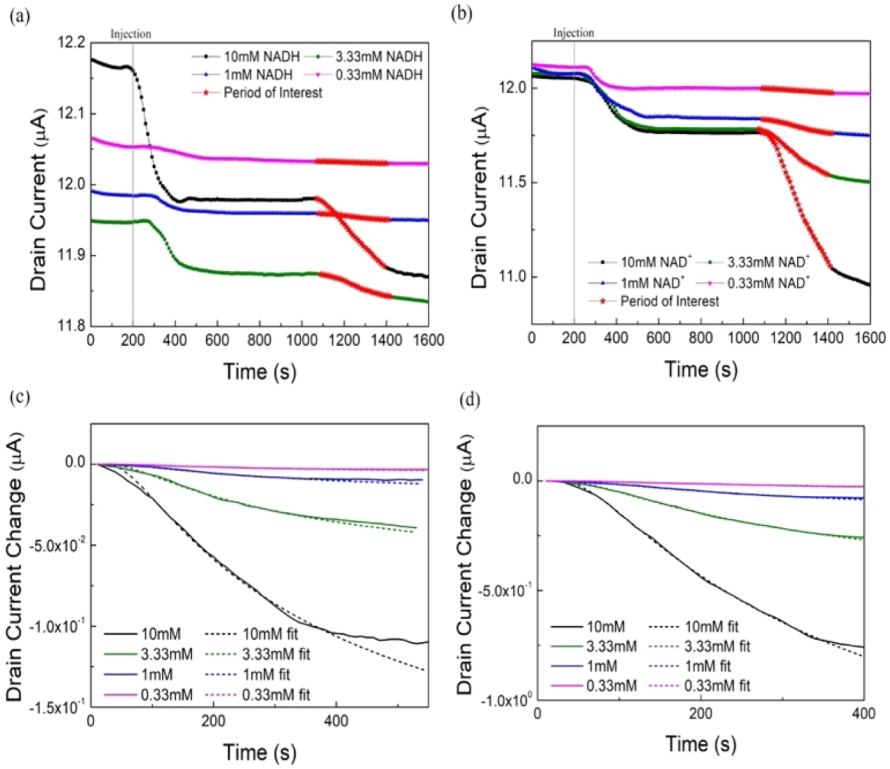

Figure 2. (a) Transient drain current responses of NADH solutions of different concentrations. (b) Transient drain currents of NAD$^+$ solutions of different concentrations. Note that those marked in red are the POI. (c) Curve fitting of NADH in the POI. (d) Curve fitting of NAD$^+$ in the POI.

https://doi.org/10.1021/acsomega.1c00222
ACS Omega 2021, 6, 11911−11917

molecules are immobile on the sensing pad, they attract opposite charges that are fixed in the upper channel, resulting in the decease of drain current.[18] To indicate the time interval where electric charges carried by the analyte are sensed, the starting and ending points are defined as the time the current slope changes beyond a certain average. Judging from the results in Figure 2a,b, the slope of the point of interest is defined to be 40% higher or lower than the average of previous at most 20 points of the same stage. Based on the definition, the arrived time of NADH and NAD^+ is around 1000−1200 s, as shown in Figure 2a,b.

To formulate the drain current response of NADH and NAD^+ at different concentrations, we derive the one-dimensional (1D) diffusion model for the biomolecules. Assuming a 1D microfluidic channel, biomolecules diffusing in the channel are expressed as[23]

$$\frac{\partial C}{\partial t} = D\frac{\partial^2 C}{\partial x^2} \qquad t > 0;\ 0 < x < \infty \tag{1}$$

where C (mM) is the concentration of the biomaterial, t (s) is the diffusion time, D (m^2/s^{-1}) is the diffusion coefficient, and x (m) is the position in the channel. Note that $x = 0$ is the location where the solution is injected. The above equation is subject to the following initial and boundary conditions in our experiment

$$\begin{cases} C(x > 0,\ t = 0) = 0 \\ C(x = 0,\ t) = C_0 \end{cases}$$

where C_0 (mM) is the initial concentration we constantly inject the biomaterial to the channel at the inlet. Based on the boundary conditions, we obtain

$$C(x_0,\ t) = C_0 * \mathrm{Erfc}\left(\sqrt{\frac{\tau}{t}}\right);\ \tau = \frac{{x_0}^2}{4D} \tag{2}$$

where x_0 (m) is the length of the sensing pad. By assuming a linear relationship between current changes and electrical charges carried by the molecules, the drain current change after target molecules arrive at the region of interest (ROI) becomes[23]

$$I(t) = I_0 + \beta * C = I_0 + \beta * C_0 * \mathrm{Erfc}\left(\sqrt{\frac{\tau}{t}}\right) \tag{3}$$

$$\Delta I(t) = I - I_0 = \beta * C_0 * \mathrm{Erfc}\left(\sqrt{\frac{\tau}{t}}\right) = B * \mathrm{Erfc}\left(\sqrt{\frac{\tau}{t}}\right)$$

$$B = \beta * C_0 \tag{4}$$

where β is a constant and ΔI (A) is the drain current change induced by the biomolecules.

The measured drain current within the time period molecules are sensed, defined as the period of interest (POI), is fitted by eq 4. The results are shown in Figure 2c,d. Parameters extracted, such as constant B and τ, are shown in Table 1. From eq 2, since the length of the sensing pad and the diffusion coefficient remain the same under different concentrations,[24] τ should be the same, which agrees with the results extracted in Table 1. Because the parameters are extracted from the drain current profile of each concentration, by correlating the constant B to the initial concentration C_0, as plotted in Figure 3, β can be obtained for both NADH and NAD^+. By plugging in the values in Table 1, the functions of drain current change of NADH and NAD^+ are expressed as

Table 1. Values of Parameters for Fitting Drain Current Responses of NADH and NAD^+ Molecules of Different Concentrations

solution concentration C_0 (mM)	B of NADH (mA/M)	B of NAD^+ (mA/M)	τ of NADH (s)	τ of NAD^+ (s)
10	−0.288	−2.245	161.64	169.67
3.33	−0.096	−0.738	160.73	164.38
1	−0.028	−0.233	169.10	163.68
0.33	−0.009	−0.070	163.37	162.87

$$\Delta I_{\mathrm{NADH}}(t) = 3.52 \times 10^{-10} - 2.89 \times 10^{-8} \times C_0 \mathrm{Erfc}\left(\sqrt{\frac{163.71}{t}}\right) \tag{5}$$

$$\Delta I_{\mathrm{NAD^+}}(t) = 4.27 \times 10^{-10} - 2.24 \times 10^{-7} \times C_0 \mathrm{Erfc}\left(\sqrt{\frac{165.15}{t}}\right) \tag{6}$$

In addition to predicting the diffusion behavior, the concentration of the biomolecules can be determined by fitting eqs 5 and 6 to the measured drain current. Under the same concentration, NAD^+ has a higher drain current decrement than NADH over the POI, which indicates that NAD^+ has higher net charges than NADH.[16]

2.3. Determination of the Apparent Equilibrium Constant of NADH−OAA Reaction. With the knowledge of the correlation between the concentration of NADH and NAD^+ and the transient drain current responses, the kinetics of the following biochemical reaction is next analyzed

$$\mathrm{NADH} + \mathrm{H^+} + \text{oxaloacetate} \overset{\mathrm{MDH}}{\Longleftrightarrow} \mathrm{NAD^+} + \text{malate} \tag{7}$$

Since the mixture of NADH and OAA involves the dynamic change of OAA in the TFT biosensor, before characterizing the reaction, the drain current response of OAA was first analyzed. An example of 10 mM OAA is shown in Figure 4. We observe an increase of current at the time around 1250 s, which will be considered as the arrival time of OAA molecules to the ROI for the subsequent experiment.

To extract the equilibrium constant of the reaction, we prepared four different solutions {i.e., 10 mM NADH + 10 mM OAA + 80 units/mL MDH [denoted as solution (1)], 3.33 mM NADH + 3.33 mM OAA + 26.6 units/mL MDH [solution (2)], 1 mM NADH + 1 mM OAA + 8 units/mL MDH [solution (3)], 0.33 mM NADH + 0.33 mM OAA + 2.66 units/mL MDH [solution (4)]}, with all premixed in separate microcentrifuges for 30 min before applying to the microfluidic channel. In the solutions, the unit of MDH implies the conversion of 1 μmole of NADH and OAA to NAD^+ and malate per minute at pH of 7.5 and a temperature of 25 °C. In our case, the amount of MDH mixed in each solution is sufficient to ensure a complete reaction.

The transient drain current responses of the premixed solutions are shown in Figure 5a. Among the curves, the first turning point occurs at the time around 1050−1100 s, which, as compared with the drain current profiles in Figure 2a,b, corresponds to the starting point of NADH and NAD^+. For the

https://doi.org/10.1021/acsomega.1c00222
ACS Omega 2021, 6, 11911−11917

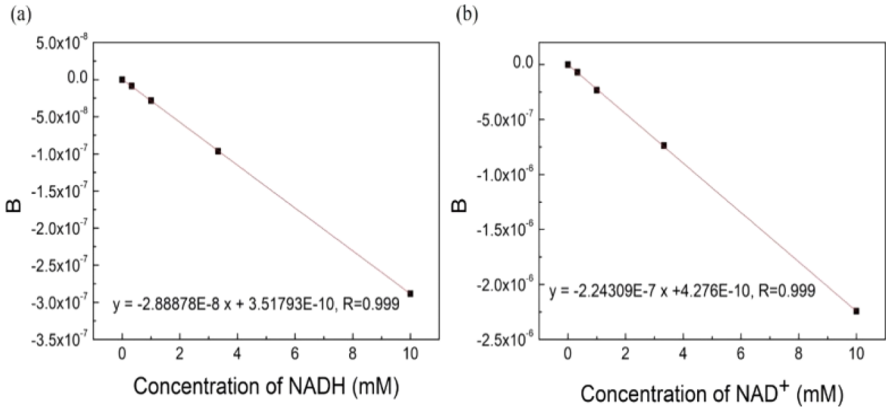

Figure 3. (a) Correlation of B and the concentration of NADH; (b) Correlation of B and the concentration of NAD^+. The equation of the correlation is shown in the figure.

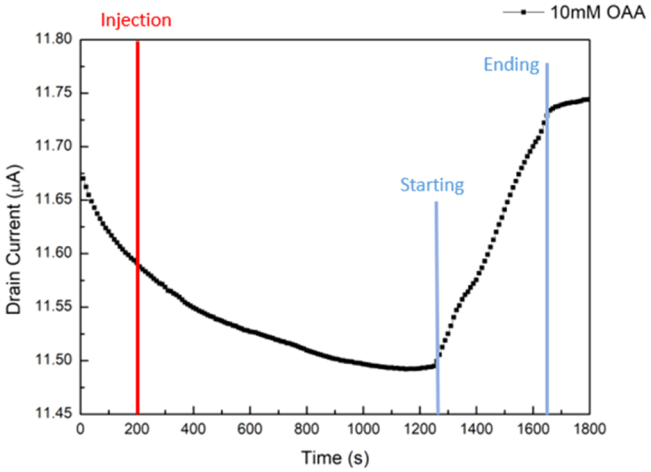

Figure 4. Transient drain current response when injecting 10 mM of OAA into the microfluidic channel.

mixture with a higher concentration of reagents, such as solution (1) or (2), a second turning point is observed around t = 1250 s, which is attributed to the detection of OAA molecules. When more OAA molecules are detected, the drain current starts to increase. Within the time interval where only NADH and NAD^+ are detected, by taking eqs 5 and 6 into consideration, the drain current of the mixture is expressed as

$$\Delta I_{mix}(t) = 3.52 \times 10^{-10} - 2.89 \times 10^{-8} \times C_{0\text{-NADH}} (1-p)\mathrm{Erfc}\left(\sqrt{\frac{163.71}{t}}\right) + 4.27 \times 10^{-10} - 2.24 \times 10^{-7} \times C_{0\text{-NADH}} p\mathrm{Erfc}\left(\sqrt{\frac{165.15}{t}}\right) \quad (8)$$

where $C_{0\text{-NADH}}$ (mM) is the initial concentration of NADH in the solution and p is the proportion of NADH converted to NAD^+. Equation 8 was employed to fit the transient response of drain current within the POI. The fitting results are shown in Figure 5b, where the starting point is defined as t = 0. The values of p extracted at different mixtures are summarized in Table 2. The ratio of NAD^+ to NADH is expressed as

$$\frac{[NAD^+]}{[NADH]} = \frac{p}{1-p} \quad (9)$$

Table 2. Ratio of NAD^+ to NADH and Apparent Equilibrium Constant K'_{eq} of Various Mixtures

solution	NAD^+/NADH	K'_{eq}
(1)	279.11	7.79×10^4
(2)	286.36	8.20×10^4
(3)	299.30	8.96×10^4
(4)	270.00	7.29×10^4

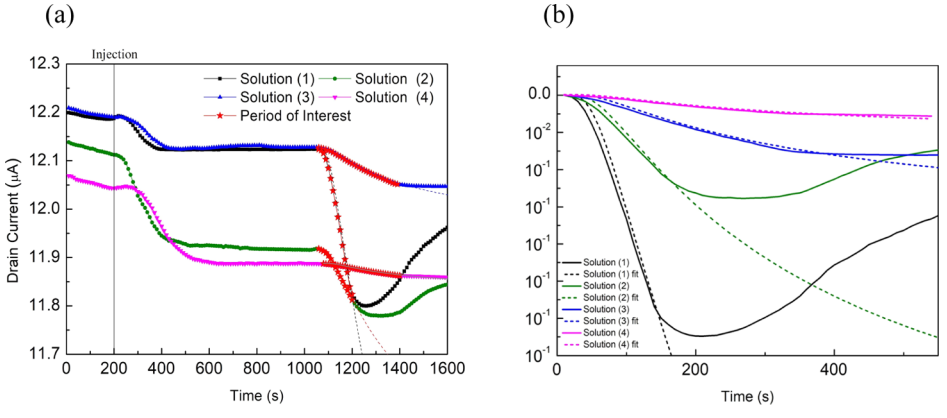

Figure 5. (a) Transient drain current responses of various mixtures and (b) corresponding fitting curves in the POI.

https://doi.org/10.1021/acsomega.1c00222
ACS Omega 2021, 6, 11911−11917

The ratio is shown in Table 2. Furthermore, the apparent equilibrium constant K'_{eq} is obtained by the following correlation

$$K'_{eq} = \frac{[NAD^+][MAL]}{[NADH][OAA]} \quad (10)$$

Ideally, the stoichiometric number of both NADH and OAA is 1, which implies that the amount of OAA converted to malate is the same as that of NADH converted to NAD^+. Therefore, the apparent equilibrium constant can be expressed as

$$K'_{eq} = \left(\frac{[NAD^+]}{[NADH]}\right)^2 = \left(\frac{p}{1-p}\right)^2 \quad (11)$$

Based on eq 11, the apparent equilibrium constants of various solutions are shown in Table 2. For comparisons, Table 3 summarizes K'_{eq} values of NADH−OAA reaction reported using various methods. The apparent equilibrium constant we obtained is slightly lower than the database value[25] but is within the range from other reports.[26,27] Traditionally, the method for detecting the NADH−OAA reaction relies on the unique optical absorption property of NADH at the wavelength of 340 nm.[28] However, since the existence of NAD^+ is optically undetectable, the optical absorption method may not be suitable for the quantitative determination of reaction species.[28] For our approach, once the correlation between reagent concentration and the drain current response profile is established, the apparent equilibrium constant of different mixtures can be determined.

Table 3. Comparisons of the Apparent Equilibrium Constant, K'_{eq}, of NADH−OAA Reaction Reported in the Literature and This Work

method	K'_{eq}
eQuilibrator[25]	1.85×10^5
optical absorbance spectrophotometer[26]	9.80×10^4
optical absorbance spectrophotometer[27]	4.72×10^4
this work	$(8.06 \pm 0.61) \times 10^4$

The parameters explored in this work, such as the ratio of NAD^+ to NADH and the equilibrium constant, are the key to the investigation of biochemical reactions, especially for discovering the metabolism mechanism. The IGZO-TFT biosensor as proposed in this work can effectively monitor biochemical reactions. By analyzing multiple drain current points in the time domain, the proposed diffusion model is less sensitive to background instability that typical transistor sensors may encounter. Even though the lack of cross-linkers limits the minimum concentration that can be detected (limit of detection) in the reaction, our approach avoids labeling or immobilization of the target protein. It has the advantage of maintaining the molecular structure of the protein so that the properties of the molecules are not altered during the reaction. Also, the TFT and microfluidic channels can be mass-manufactured in an array form, which is a high-throughput method in detecting biochemical reactions.

3. MATERIALS AND METHODS

3.1. Device Design and Fabrication. The TFT-microfluidic channel biosensor is shown in Figure 6, along with a microscopic image of the TFT image. The TFT and microfluidic channel were fabricated on the separate glass substrate; both are connected by Au bond wires. We employed a dual-gate IGZO TFT (see Figure 7) as the transducer to convert biological signals into electric signals and the microfluidic channel for biomolecular diffusion. The detailed device fabrication steps for IGZO TFTs and fluidic channels have been described elsewhere.[16,17] The microfluidic channel is composed of one inlet and one outlet with a diameter of 6.1 mm. The dimensions of the fluidic channel are 14, 1, and 1 mm in length (including the 6.1 mm diameter inlet), width, and height, respectively.

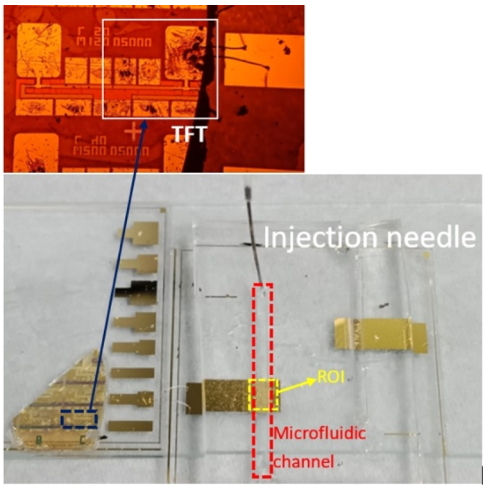

Figure 6. Biosensor employed in this work for monitoring biochemical reaction. The sensor is composed of a TFT in the left and a microfluidic channel in the right. ROI is located on the Au sensing pad, which is connected to the top gate through Au bond wires.

3.2. Operation Principle and Measurements. The concentration of target molecules is determined by the amount of electrical charges carried. The TFT detects charges and converts them to the drain current for readout. In our device, the bottom gate (see Figure 7) provides bias voltage and regulates the operating drain current in the saturation region. It also acts as a reference electrode for the transistor sensor. As schematically shown in Figure 7, with the diffusion of target molecules in the microfluidic channel, the negative electrical charges carried by the molecules will be sensed in the ROI and deplete electrons in the TFT channel through the Au wire. The drain current will be changed correspondingly.

In this work, the biomolecules, NADH, NAD^+, OAA, and MDH, were diluted in 0.01 × PBS (pH = 7.4) to obtaine the desired concentration. The drain−source voltage, V_{DS}, of 5 V and the bottom gate−source voltage, V_{GS}, of 10 V, were provided to the TFT during measurement. The sample rate is 10 s. Since the whole experimental setup is sensitive to the static charges in the environment and the TFT current can be perturbed during the solution injection to the microfluidic channel, before characterizing biochemical reactions, we conducted two types of test runs to understand the stress behavior of the TFT device and the interference on drain current when the solution was injected. First, with the microfluidic channel prefilled with only PBS (without any target molecules), the transient TFT current was recorded. Second, the drain current response of injecting only the buffer (0.01 × PBS) (without any target molecules) to the

https://doi.org/10.1021/acsomega.1c00222
ACS Omega 2021, 6, 11911−11917

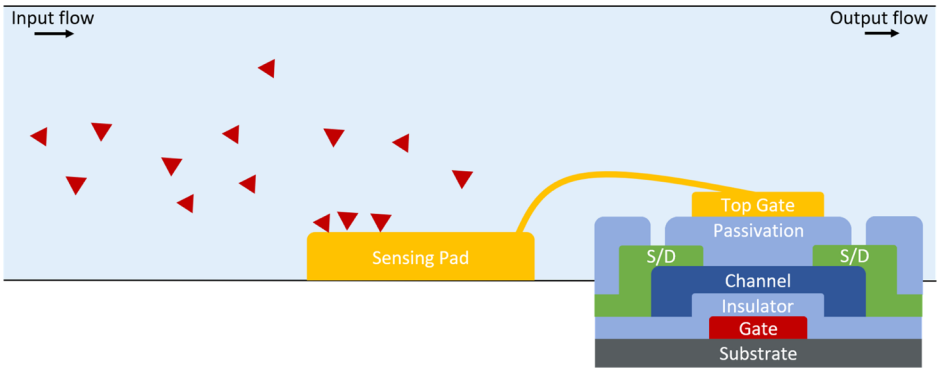

Figure 7. Illustration of the diffusion of target molecules in the microfluidic channel. The electrical charges carried by the molecules above the Au sensing pad will be detected by the TFT.

microfluidic channel prefilled with 14 μL of the buffer was analyzed.

To characterize biochemical reactions, we first calibrated current responses of pure NADH and NAD^+ solutions. The concentrations of NADH and NAD^+ selected in this work are 10, 3.33, 1, and 0.33 mM. The transient drain current profiles were fitted following the diffusion equation to correlate the concentration of the target analyte with the current change. Second, the reaction kinetics of NADH and OAA was investigated by monitoring the diffusion behavior of the mixture. We then determined the amount of NADH molecules converted to NAD^+ so that the equilibrium constant of the bioreaction was derived.

4. CONCLUSIONS

In this work, a molecular diffusion model was demonstrated to extract parameters of the biochemical reaction without labeling and forehanded protein immobilization. Using the reaction between NADH and OAA with the catalyst MDH as an example, correlation between the diffusion model and the time-domain drain current profile of biomaterials was established so that the function for determining reactants and products can be derived. The ratio of NAD^+ to NADH and the equilibrium constant, K_{eq}, $(8.06 \pm 0.61) \times 10^4$, are comparable to other approaches in the literature. Our method avoids determining the molecular concentration based solely on the absolute current variation as in the previous works. Thus, more reliable results that mitigate background instabilities can be obtained. Since the microfluidic channels and TFTs were fabricated based on the semiconductor process procedure, the determination of biochemical characteristics of various solutions using our method can be conducted in a parallel manner. Our sensors have the potential to be applied to the pharmaceutical industry which requires high-throughput measurements.

AUTHOR INFORMATION

Corresponding Author

Jian-Jang Huang − *Graduate Institute of Photonics and Optoelectronics, National Taiwan University, Taipei 106, Taiwan; Department of Electrical Engineering, National Taiwan University, Taipei 10617, Taiwan;* orcid.org/0000-0002-5761-2177; Email: jjhuang@ntu.edu.tw

Authors

Yao-Hsuan Lai − *Graduate Institute of Photonics and Optoelectronics, National Taiwan University, Taipei 106, Taiwan*

Jin-Chun Lim − *Graduate Institute of Photonics and Optoelectronics, National Taiwan University, Taipei 106, Taiwan*

Ya-Chu Lee − *Graduate Institute of Photonics and Optoelectronics, National Taiwan University, Taipei 106, Taiwan*

Complete contact information is available at: https://pubs.acs.org/10.1021/acsomega.1c00222

Notes

The authors declare no competing financial interest.

ACKNOWLEDGMENTS

This work was supported by the Ministry of Science and Technology, Taiwan (grant number: 108-2221-E-002-014-MY3).

ABBREVIATIONS

TFT, thin-film transistor; NADH, nicotinamide adenine dinucleotide, reduced form; OAA, oxaloacetic acid, the conjugate acid of oxaloacetate; MDH, malate dehydrogenase; IGZO, indium−gallium−zinc oxide; PBS, phosphate-buffered saline; ROE, region of interest; 1D, one-dimensional; POI, period of interest

REFERENCES

(1) Reddy, V. N.; Liebman, M. N.; Mavrovouniotis, M. L. Qualitative analysis of biochemical reaction systems. *Comput. Biol. Med.* **1996**, *26*, 9−24.

(2) Keusgen, M. Biosensors: new approaches in drug discovery. *Naturwissenschaften* **2002**, *89*, 433−444.

(3) Lahti, J. L.; Tang, G. W.; Capriotti, E.; Liu, T.; Altman, R. B. Bioinformatics and variability in drug response: a protein structural perspective. *J. R. Soc., Interface* **2012**, *9*, 1409−1437.

(4) Schilling, E. A.; Kamholz, A. E.; Yager, P. Cell lysis and protein extraction in a microfluidic device with detection by a fluorogenic enzyme assay. *Anal. Chem.* **2002**, *74*, 1798−1804.

(5) Hasan, A.; Nurunnabi, M.; Morshed, M.; Paul, A.; Polini, A.; Kuila, T.; Al Hariri, M.; Lee, Y.-k.; Jaffa, A. A. Recent Advances in Application of Biosensors in Tissue Engineering. *BioMed Res. Int.* **2014**, *2014*, 307519.

(6) Chang, I. S.; Jang, J. K.; Gil, G. C.; Kim, M.; Kim, H. J.; Cho, B. W.; Kim, B. H. Continuous determination of biochemical oxygen

demand using microbial fuel cell type biosensor. *Biosens. Bioelectron.* **2004**, *19*, 607−613.
(7) Kudo, H.; Sawai, M.; Suzuki, Y.; Wang, X.; Gessei, T.; Takahashi, D.; Arakawa, T.; Mitsubayashi, K. Fiber-optic bio-sniffer (biochemical gas sensor) for high-selective monitoring of ethanol vapor using 335nm UV-LED. *Sens. Actuators, B* **2010**, *147*, 676−680.
(8) Monsigny, M.; Petit, C.; Roche, A.-C. Colorimetric determination of neutral sugars by a resorcinol sulfuric acid micromethod. *Anal. Biochem.* **1988**, *175*, 525−530.
(9) Spencer, K. Analytical Reviews in Clinical Biochemistry: The Estimation of Creatinine. *Ann. Clin. Biochem.* **1986**, *23*, 1−25.
(10) Park, I.; Li, Z.; Li, X.; Pisano, A. P.; Williams, R. S. Towards the silicon nanowire-based sensor for intracellular biochemical detection. *Biosens. Bioelectron.* **2007**, *22*, 2065−2070.
(11) Syu, Y.-C.; Hsu, W.-E.; Lin, C.-T. Review-Field-Effect Transistor Biosensing: Devices and Clinical Applications. *ECS J. Solid State Sci. Technol.* **2018**, *7*, Q3196−Q3207.
(12) Vu, C.-A.; Chen, W.-Y. Field-Effect Transistor Biosensors for Biomedical Applications: Recent Advances and Future Prospects. *Sensors* **2019**, *19*, 4214.
(13) Sadighbayan, D.; Hasanzadeh, M.; Ghafar-Zadeh, E. Biosensing based on field-effect transistors (FET): Recent progress and challenges. *TrAC, Trends Anal. Chem.* **2020**, *133*, 116067.
(14) Yang, T.-H.; Chen, T.-Y.; Wu, N.-T.; Chen, Y.-T.; Huang, J.-J. IGZO-TFT Biosensors for Epstein-Barr Virus Protein Detection. *IEEE Trans. Electron Devices* **2017**, *64*, 1294−1299.
(15) Wu, N.-T.; Jiang, B.-S.; Lo, Y.-H.; Huang, J.-J. Investigation of streptavidin-ligand biochemical interactions by IGZO thin film transistors integrated with microfluidic channels. *Sens. Actuators, B* **2018**, *262*, 418−424.
(16) Wang, Y.-W.; Chen, T.-Y.; Yang, T.-H.; Chang, C.-C.; Yang, T.-L.; Lo, Y.-H.; Huang, J.-J. Thin-Film Transistor-Based Biosensors for Determining Stoichiometry of Biochemical Reactions. *PLoS One* **2016**, *11*, No. e0169094.
(17) Chen, T.-Y.; Yang, T.-H.; Wu, N.-T.; Chen, Y.-T.; Huang, J.-J. Transient analysis of streptavidin-biotin complex detection using an IGZO thin film transistor-based biosensor integrated with a microfluidic channel. *Sens. Actuators, B* **2017**, *244*, 642−648.
(18) Chou, C.-H.; Lim, J.-C.; Lai, Y.-H.; Chen, Y.-T.; Lo, Y.-H.; Huang, J.-J. Characterizations of protein-ligand reaction kinetics by transistor-microfluidic integrated sensors. *Anal. Chim. Acta* **2020**, *1110*, 1−10.
(19) Mettler, I. J.; Beevers, H. Oxidation of NADH in glyoxysomes by a malate-aspartate shuttle. *Plant Physiol.* **1980**, *66*, 555−560.
(20) Borst, P. The malate-aspartate shuttle (Borst cycle): How it started and developed into a major metabolic pathway. *IUBMB Life* **2020**, *72*, 2241−2259.
(21) Cho, I.-T.; Lee, J.-M.; Lee, J.-H.; Kwon, H.-I. Charge trapping and detrapping characteristics in amorphous InGaZnO TFTs under static and dynamic stresses. *Semicond. Sci. Technol.* **2008**, *24*, 015013.
(22) Dunphy-Guzman, K. A.; Karnik, R. N.; Newman, J. S.; Majumdar, A. Spatially controlled microfluidics using low-voltage electrokinetics. *J. Microelectromech. Syst.* **2006**, *15*, 237−245.
(23) John, C. Emeritus Professor John Crank, *The Mathematics of Diffusion*; Clarendon Press, 1979.
(24) Segato, T. P.; Coltro, W. K. T.; de Jesus Almeida, A. L.; de Oliveira Piazetta, M. H.; Gobbi, A. L.; Mazo, L. H.; Carrilho, E. A rapid and reliable bonding process for microchip electrophoresis fabricated in glass substrates. *Electrophoresis* **2010**, *31*, 2526−2533.
(25) Flamholz, A.; Noor, E.; Bar-Even, A.; Milo, R. eQuilibrator–the biochemical thermodynamics calculator. *Nucleic Acids Res.* **2012**, *40*, D770−D775.
(26) Dasika, S. K.; Vinnakota, K. C.; Beard, D. A. Determination of the catalytic mechanism for mitochondrial malate dehydrogenase. *Biophys. J.* **2015**, *108*, 408−419.
(27) Guynn, R. W.; Gelberg, H. J.; Veech, R. L. Equilibrium constants of the malate dehydrogenase, citrate synthase, citrate lyase, and acetyl coenzyme A hydrolysis reactions under physiological conditions. *J. Biol. Chem.* **1973**, *248*, 6957−6965.
(28) Paul, H. *Determination of NADH Concentrations with the Synergy 2 Multi-Detection Microplate Reader Using Fluorescence or Absorbance*; BioTek Instruments, 2007.

https://doi.org/10.1021/acsomega.1c00222
ACS Omega 2021, 6, 11911−11917